Nat. Hazards Earth Syst. Sci. Discuss., https://doi.org/10.5194/nhess-2018-64
Manuscript under review for journal Nat. Hazards Earth Syst. Sci.
Discussion started: 26 March 2018

Natural Hazards and Earth System Sciences
Discussions

Atmospheric Circulation Changes and their Impact on Extreme Sea Levels around Australia

Frank Colberg[1], Kathleen L. McInnes[2], Julian O'Grady[2], Ron K. Hoeke[2]

[1]Australia Bureau of Meteorology, Melbourne VIC 3001, Australia
[2]Climate Science Centre, CSIRO Marine and Atmospheric Research Aspendale, 3195, Australia

Correspondence to: K. McInnes (Kathleen.mcinnes@csiro.au)

Abstract. Projections of sea level rise (SLR) will lead to increasing coastal impacts during extreme sea level events globally, however, there is significant uncertainty around short-term coastal sea level variability and the attendant frequency and severity of extreme sea level events. In this study, we investigate drivers of coastal sea level variability (including extremes) around Australia by means of historical conditions as well as future changes under a high greenhouse gas emissions scenario (RCP 8.5). To do this, a multi-decade hindcast simulation is validated against tide gauge data. The role of tide-surge interaction is assessed and found to have negligible effects on storm surge characteristic heights over most of the coastline. For future projections, twenty-year long simulations are carried out over the time periods 1981-1999 and 2081-2099 using atmospheric forcing from four CMIP5 climate models. Results provide insights into how future atmospheric circulation changes may impact Australia's coastal zone and highlight regions of potential sensitivity to atmospheric circulation changes. Areas of note are the Gulf of Carpentaria in the north where changes to the northwest monsoon could lead to relatively large increases in extreme sea levels during Austral summer. For the southern mainland coast the simulated scenarios suggest that a southward movement of the subtropical ridge leads to a small reduction in sea level extremes.

1 Introduction

Extreme sea levels (ESLs) are a significant hazard for many low-lying coastal communities [*Hanson et al.*, 2011; *Nicholls et al.*, 2011] and with rising global mean sea level extreme events are expected to rise [*Menéndez and Woodworth*, 2010]. ESLs are largely driven by the combination of the storm surge with astronomical tides (storm tides), but are also influenced by larger-scale atmospheric and oceanic circulation patterns. It is therefore important to understand how projected changes to atmospheric and ocean circulation and severe storms may influence the frequency and intensity of ESLs as well as considering projected sea level rise (SLR).

ESL hazards are typically represented as probability-based exceedance levels with uncertainties associated to it. These uncertainties may be significantly larger than uncertainties in projected SLR itself [*Wahl et al.,* 2017]. Many studies have attempted to quantify ESL uncertainties using historical tide gauge information combined with global SLR projections [e.g. *Hunter, et al*., 2013], or by spatially extrapolating tide gauge observations using a hydrodynamic model [e.g. *Haigh et al*., 2014a]. In the present study, we assess the performance of a hydrodynamic model for the Australian region and examine atmospheric drivers of ESL and how they may change under future climate conditions.

A number of studies have used a similar approach, i.e. investigating ESL changes using hydrodynamic models forced by global climate models (GCMs) or regional climate models (RCMs). Lowe et al. [2009] developed projections of storm surge change for the UK using climate forcing from an 11-member perturbed physics ensemble of the Hadley Centre GCM downscaled to 25 km resolution with the RCM HadRM3 [*Murphy et al.*, 2007] under a mid-range SRES

Nat. Hazards Earth Syst. Sci. Discuss., https://doi.org/10.5194/nhess-2018-64
Manuscript under review for journal Nat. Hazards Earth Syst. Sci.
Discussion started: 26 March 2018

Natural Hazards and Earth System Sciences Discussions

[*Nakićenović and Swart*, 2000] emission scenario. Results indicated that the changes in the 2 to 50-year storm surge height associated with projected changes in weather and storms would increase by no more than 0.09 m by 2100 anywhere around the UK coast. [*Sterl et al.*, 2009] concatenated the output from a 17-member ensemble of a mid-range SRES emissions scenario from the ECHAM5/MPI-OM climate model [*Jungclaus et al.*, 2006] to estimate 10,000-year return values of surge heights along the Dutch coastline. No statistically significant change in this value was projected for the 21st century because projected wind speed changes were associated with non-surge generating south westerlies rather than surge-conducive northerlies. In southern Europe, *Marcos et al.* [2011] assessed changes in storm surges in the Mediterranean Sea and Atlantic Iberian coasts using climate model forcing from the ARPEGE-v3 global, spectral stretched-grid climate model under a high, medium and low SRES emissions scenario [*Jordà et al.*, 2012]. Findings revealed a general decrease in both the frequency and magnitude of storm surges with up to a 0.08 m reduction in the 50-year return levels. In southern Australia *Colberg and McInnes* [2012] found both positive and negative changes in 95th percentile sea level height across the southern half of the Australian continent in surge model simulations forced by the high SRES emission scenario of the CSIRO Mark 3.5 GCM [*Gordon et al.*, 2010] and two simulations of the CCAM stretched grid global model [*McGregor and Dix*, 2008]. The ESL changes were small, mostly negative along the southern mainland coast but with wintertime increases over Tasmania. These resembled the changes in wind patterns to some degree, although there were large inter-model differences.

Several studies have also examined the non-linear effect of rising sea levels on tide and surge propagation. Using a global tide model, Pickering [2017] found that changes in mean high tide levels exceeded ±10% of the SLR at approximately 10% of coastal cities when coastlines were held fixed, but a reduction of tidal range when coastlines were allowed to recede due to resulting changes in the period of oscillation. Arns et al. [2015] investigated the non-linear impact of SLR on maximum storm surge heights in the North Sea, focussing on the German Bight. They found that maximum storm surges relative to the imposed background sea levels were amplified by up to 20% when the background mean sea levels were elevated by around 0.5 m. The positive increases in extreme water levels were caused by nonlinear changes in the tidal component, which were only partially offset by a reduction in the storm surge component.

Recent studies have also been undertaken for locations that experience tropical cyclones. For example, *Unnikrishnan et al.* [2011] used RCM simulations to force a storm-surge model for the Bay of Bengal and found that the combined effect of mean SLR of 4 mm yr^{-1} and RCM projections for the high emissions scenario (2071– 2100) gave an increase in 1-in-100 year heights in the range of 15–20% compared to the 1961–1990 baseline. For east Asia, *Yasuda et al.* [2014] applied a hydrodynamic model based on a 20-km resolution climate model. Storm surge heights increased in the future for much of the coastline considered. For New York, Lin et al. [2012] investigated the change in extreme sea levels arising from hurricanes over 2081-2100 relative to 1981-2000 in four GCMs run with the SRES medium emission scenario by generating synthetic cyclones under the background conditions provided by the GCMs. Accounting for hurricane forcing only, results differed markedly between the four climate models ranging from overall increases to decreases in storm surge level. McInnes et al. [2014, 2015] used a synthetic cyclone technique to investigate the effect of a 10% increase in cyclone intensity and a frequency reduction of 25% on storm tides over Fiji and Samoa and found a reduction in storm tides with return periods of less than 50 years and an increase for return periods longer than 200 years.

Numerical modelling studies of the non-linear interactions between sea level rise and cyclone-induced extreme water levels due to tides, storm surge and waves have also been undertaken. Smith et al. [2010] showed that sea level rise altered the speed of propagation of tropical cyclone-induced storm surges on the south-eastern Louisiana coast and amplified the extreme water levels under SLR although the amount of amplification varied significantly along different

Nat. Hazards Earth Syst. Sci. Discuss., https://doi.org/10.5194/nhess-2018-64
Manuscript under review for journal Nat. Hazards Earth Syst. Sci.
Discussion started: 26 March 2018

Natural Hazards and Earth System Sciences Discussions

parts of the coast. Hoeke et al. [2015] found that SLR reduced wave setup and wind setup by 10-20% but increased wave energy reaching the shore by up to 200% under cyclone conditions along the Apia, Samoa coastline.

Australia extends from the tropics to the mid-latitudes with a variety of meteorological systems responsible for extreme sea levels along its coastline [*McInnes et al.*, 2016]. The range of weather systems, and more particularly their associated spatial scales means that it is challenging to obtain meteorological forcing that consistently represents all weather systems responsible for sea level extremes.

Haigh et al., [2014a; 2014b] modelled ESLs in Australia using two approaches. In Haigh et al., 2014a t the water levels arising from weather and tides were investigated over the period 1949 to 2009 using 6-hourly meteorological forcing obtained from the NCEP reanalyses while in Haigh et al., 2014b ESLs were simulated using a synthetic cyclone approach. As expected, extreme sea levels over the tropical northern coastlines were underestimated in the first study compared to the second one because of the low resolution of tropical cyclones in the reanalysis data set.

The present study assesses the performance of a medium resolution hydrodynamic model for the Australian region to investigate ESLs for the current climate and examine potential changes in a future climate scenario. The model described by *Colberg and McInnes* [2012] is extended to cover the entire Australian coastline at 5 km resolution. A current climate (baseline) simulation is undertaken with tide and atmospheric forcing over the period 1981-2012 using reanalyses from the NCEP Climate Forecast System Reanalyses (CFSR) [*Saha et al.*, 2010]. The performance of the model is assessed with respect to tides, weather driven sea levels, and tide-surge interaction. Finally, changes are investigated in storm surge and seasonal sea levels around the coastline based on forcing from an ensemble of four CMIP5 models forced with the RCP 8.5 emission scenario [*Taylor et al.*, 2012].

The paper is organised as follows. Section 2 describes the model setup, input data sets and procedure for assessing model performance. Section 3 assesses the model performance and the baseline simulations are used to investigate tide-surge interaction around the Australian coastline and the meteorological causes of ESLs. Section 4 presents the results from simulations forced by climate models and section 5 discusses the results, conclusions and further work.

.

2 Model Description and Method

2.1 Model Configuration

As with Colberg and McInnes [2012], the model used in this study is the Rutgers version of the Regional Ocean Modeling System (ROMS) [Shchepetkin and McWilliams, 2005] configured to run in barotropic or 'depth-averaged' mode. The model grid spans the region shown in Figure 1 at 5 km resolution. Bathymetry for the model is obtained from the 1'□1' resolution General Bathymetric Chart of the Oceans [GEBCO, Jakobsson, et al., 2008] data set.

For simulations including tides, the tidal currents and heights were derived from the TPXO7.2 global model (Egbert et al., 1994; Egbert and Erofeeva, 2002) and applied to the open model boundaries. TPXO7.2 best fits (in a least-squares sense) the Laplace Tidal Equations and along track-averaged data from the TOPEX/Poseidon and Jason altimetry missions, obtained with OTIS (Oregon State University Tidal Inversion Software). Eight primary tidal constituents (M2, S2, N2, K2, K1, O1, P1, Q1) are provided on a 1/4 of a degree resolution full global grid. A combination of Flather/Chapman boundary conditions was used in applying the tidal forcing [Flather, 1976; Chapman, 1985]. The Flather condition was applied to the normal component of the barotropic velocity and radiates deviations from the values at exterior grid points out of the model domain at the speed of the external gravity waves. The corresponding Chapman

Nat. Hazards Earth Syst. Sci. Discuss., https://doi.org/10.5194/nhess-2018-64
Manuscript under review for journal Nat. Hazards Earth Syst. Sci.
Discussion started: 26 March 2018

Natural Hazards and Earth System Sciences Discussions

condition for surface elevation assumes all outgoing signals leave at the shallow-water wave speed. Meteorological forcing is discussed in the next section.

2.2 Baseline experiment

In the first part of the study, we assess the ability of the Australia-wide ROMS model to simulate historical tides and meteorologically-driven water levels. The model experiments performed are also used to investigate non-linear tide-surge interactions as well as the meteorological causes of extreme sea levels around the Australian coastline. Three baseline experiments are run over the period 1981-2012. The first experiment, B-TM, includes tidal and meteorological forcing, the second, B-T, tide-forcing only and the third, B-M, meteorological forcing only. Meteorological forcing for these experiments is obtained from the Climate Forecast System Reanalyses (CFSR) dataset [Saha et al., 2010, Saha et al., 2014], which provides meteorological variables across the globe at hourly temporal resolution and approximately 38 km spatial resolution from 1979 to 2012.

2.3 Climate change experiments

Finally, a set of simulations with meteorological forcing from four GCMs from the 5th Phase of the Coupled Model Intercomparison Project (CMIP5; [Taylor et al, 2012]) is undertaken to assess how climate change will affect sea levels around the Australian coast. The various experiments are described in Table 1. The models were chosen by subjectively evaluating performance metrics reported by Hemer & Trenham [2016], computational considerations and data availability.

Tides were not included in the simulations forced by climate models. This was primarily because of the large computational overhead required to undertake two simulations for each time slice (current and future) consisting of one simulation with tides only and one with tides and atmospheric forcing in order to calculate non-tidal residuals. Furthermore, we note that the convention of some climate modelling centres to run climate models on non-standard yearly cycles (e.g. 360 days in the case of the HadGem model) means that the applications of astronomical tides is non-trivial. As will be discussed in section 3.3, the decision to omit tidal forcing from the climate runs is somewhat justified because non-linear tide surge interaction is evident around parts of Australia and therefore may impact substantially on an individual surge event it does not change the surge statistics over a period of years to decades [*Williams et al.,* 2016], which is the main focus of the experiments. In the following we refer to the climate change simulations as CC (see also Table 1).

3 Baseline results and model performance

Here we assess the baseline experiments (forced by CFSR and/or tides) in terms of how well the model-generated sea levels compared with observations. In the first sub-section, we address the contribution of seasonal and interannual variability in sea level in the modelled and observed data. The following sub-sections examine the performance of the model in representing astronomical tides, the high frequency variability in sea levels including extremes, and the meteorological drivers of ESLs around the coast. Finally, we examine tide-surge interaction.

Nat. Hazards Earth Syst. Sci. Discuss., https://doi.org/10.5194/nhess-2018-64
Manuscript under review for journal Nat. Hazards Earth Syst. Sci.
Discussion started: 26 March 2018

Natural Hazards and Earth System Sciences Discussions

The model is assessed against hourly tide measurements from fourteen high quality tide gauges from the Australian Base Line Sea Level Monitoring Network with data available from 1993 to 2012 (Figure 1). We decompose both the tide gauge measurements and the simulated sea levels at corresponding model grid points in the B-TM simulation into components consisting of the (a) seasonal and interannual variability, (b) the tidal signal and (c) the residual signal (the remaining signal after the removal of the seasonal and tidal components from the total sea level) using the approach of *Haigh et al.* [2014a]. First, measured sea levels are linearly de-trended at each station. A 30-day running mean is then subtracted from the de-trended measured and modelled time series. Finally the time series is de-tided by performing a harmonic analysis on the time series. using T-Tide [*Pawlowicz et al.*, 2002]. The sea level residuals, which include storm surges, are obtained after the removal of these components of the total sea level.

These component time series, as well as the total sea level, are compared by means of root mean square errors (RMSE), The mean difference in standard deviation between observations and simulation (STDE) and linear correlations between the modelled and observed time series over the period from 1993 to 2012 (the shorter assessment period is determined by the availability of tide gauge data at the selected sites). In addition, a 1-day running mean filter was applied to the de-tided modelled and observed sea levels for the locations of Darwin and Broome because these locations display high frequency intra-daily to daily variability in sea surface height after applying the filtering techniques described above. This variability may be a consequence of the large tidal signal in the area propagating over a fairly shallow and wide shelf. The nature of the high frequency variability is such that at times it would mask surge events related to atmospheric weather patterns.

3.1 Seasonal and interannual variations in sea level

Table 2 compares the differences between the seasonal signal in the observations and the model via RMSE, STDE and correlation coefficients. For most of the coastline, the RMSE values are 0.07 m or less with lowest values along the southeast coast. Higher values of RMSE occur on the northern and western coastline from Milner Bay (0.15 m) to Hillarys (0.10 m). Similarly, STDE indicate that the model underestimates the seasonal component by a larger amount in these locations. The reason for the poorer model performance in these locations may be attributed to seasonal and interannual variations since these regions feature a relatively large steric component, which is not simulated by barotropic models [*Haigh et al.*, 2014a].

In Milner Bay, a large seasonal cycle in sea level occurs in part due to the transition from the prevailing north-westerly winds during the December to April monsoon to the dry season southeasterly trade winds from May to November [*Oliver and Thompson*, 2011; *Green et al.*, 2010] and steric effects from seasonal variations in ocean temperature and salinity. Variations in barotropic and steric sea level components are approximately in phase, are at a maximum in January and are highest in the southeast of the Gulf of Carpentaria [*Forbes and Church*, 1983].

The range of the seasonal signal from tide gauge measurements for Milner Bay is estimated here to be 0.67 m. This is lower than the range of approximately 0.8 m reported in *Tregoning et al.* [2008] based on five years of data and the difference may be a result of interannual variations in the seasonal cycle in the longer record that is analysed here. The range of the seasonal signal in the barotropic model is 0.27 m, also smaller than the barotropic range of 0.4 m estimated by *Tregoning et al.* [2008]. Nevertheless, the results highlight that the steric component contributes to about half of the seasonal variation in sea levels in the Gulf of Carpentaria.

Nat. Hazards Earth Syst. Sci. Discuss., https://doi.org/10.5194/nhess-2018-64
Manuscript under review for journal Nat. Hazards Earth Syst. Sci.
Discussion started: 26 March 2018

Natural Hazards and Earth System Sciences Discussions

A relatively large steric component is also present in the seasonal signal from Darwin to Hillarys and this is related to seasonal variations in the strength of the southward flowing Leeuwin Current, which is weakest in October to March as it flows against maximum southerly winds and is strongest between April and August when southerly winds are weaker [*Godfrey and Ridgway*, 1985]. This produces an annual cycle in sea levels at Hillarys of about 0.22 m with maximum levels occurring in May-June and minimum levels in October-November [*Pattiaratchi and Eliot*, 2008]. The range of the seasonal signal from the Hillarys tide gauge is estimated here to be 0.34 m whereas in the model it is 0.09 m, the difference being of a similar order to the steric effect, which is not captured by the model.

3.2 Tides

A comparison of the amplitudes of the eight major tidal constituents derived from the measured and modelled sea levels over 1993-2012 is presented in Figure 2 for each of the tide gauge locations. For most locations there is reasonably good agreement between constituents estimates from model and observations. The largest differences in the M2 and S2 constituents occur along the south coast at Thevenard and Port Stanvac. At Port Stanvac in particular, this may be related to poor resolution of tidal waves propagating into the Gulf of St. Vincent. Milner Bay in the Gulf of Carpentaria is also showing poor agreement, with the leading O1 and K1 constituents largely underestimated by the model. The RMSE values in Table 2 also reflect larger differences and lowest correlations at Port Stanvac and Thevenard. Locations with large tidal amplitudes such as Broome and Darwin display the largest RMSE errors (30 and 40cm respectively). On average RMSE, STDE and correlation across all locations is 0.17 m, -0.05 m and 0.94 respectively indicating good model skill overall.

3.3 Sea Level Residuals

The sea level residuals, obtained after removal of the tides and seasonal signal are indicative of short-term fluctuations such as storm surge. Table 2 shows error statistics for the sea level residuals over the period 1993 to 2009 and in Figure 3 data is plotted for selected sites for the year 1997. This particular year was prominent for storm surges at many of the locations across the Australian region. The lowest RMSE errors of around 0.06 m are generally located along the east coast and within Bass Strait. The largest RMSE errors of 0.11 m are found at Milner Bay in the Gulf of Carpentaria and at Thevenard and Port Stanvac along the south coast. Correlations are highest at gauges across the south coast stretching from Hillarys to Spring Bay with values exceeding 0.8 at all locations except Burnie where a slightly lower correlation of 0.77 was found. Correlations are lowest in macro-tidal areas with large shelves and/or complex bathymetry, with the lowest values of 0.55 and 0.39 at Darwin and Broome respectively. The poorer performance in these areas are further demonstrated using quantile-quantile plots shown in Figure 4. It can be seen that the ESLs tend to be more systematically underestimated along this coastline than in the southern mid-latitudes. For example, at Milner Bay the 99.9th percentile values are underestimated by approximately 0.5 m. At Port Stanvac, the underestimation of the high percentiles is likely a result of the 5 km grid spacing of the model inadequately resolving the Gulf of St. Vincent in which Port Stanvac is located. The spatial scale of the synoptic weather systems typically responsible for causing ESLs and the degree to which the CFSR atmospheric reanalysis resolves these systems may also be a factor in the ROMS model's ability to represent storm surge.

The synoptic weather systems responsible for the storm surge events identified by arrows in Figure 3 (note that for Burnie, the synoptic map for Portland applies) are shown in Figure 5, which presents the mean sea level pressure (MSLP) and 10 m wind vectors at the time of the peak sea levels. At Spring Bay, the peak residual of 0.4 m on 8 July 1997 is associated with the passage of a frontal trough that brings low pressure and southwesterly winds along the eastern

Nat. Hazards Earth Syst. Sci. Discuss., https://doi.org/10.5194/nhess-2018-64
Manuscript under review for journal Nat. Hazards Earth Syst. Sci.
Discussion started: 26 March 2018

Natural Hazards and Earth System Sciences Discussions

Tasmanian coast (Figure 5a). *McInnes et al.* [2012] found that daily maximum sea levels at Spring Bay were highly correlated with those in Hobart (r=0.98) and Portland (r=0.80) indicating the strong influence of frontal systems on sea level extremes in this part of the country. Indeed relative peaks in residuals are evident at other south mainland coast stations for this event (Figures 5g-j).

At Port Kembla a relative peak in residual sea level of 0.3 m at around 10 May 1997 is the result of an east coast low that brings southeasterly winds to the coast. These systems are the cause of the majority of elevated sea level events along this coastline [*McInnes and Hubbert*, 2001]. A tropical cyclone off the northeast coast around 9 March (Figure 3c and 5c) and in the Gulf of Carpentaria on 28 December are responsible for sea level residuals of up to 0.4 at Rosslyn Bay and 1.0 m at Milner Bay respectively (Figure 3d and 5d). A second residual peak at Rosslyn Bay of up to 0.4 m around 13 May was not captured by the model. The cause of this peak in the observations and why the model fails to capture this peak is not clear although inspection of MSLP and wind fields around this time shows a cut-off low at latitude 30°S moving eastwards into the Tasman Sea and generating strong southeasterly winds directed towards Rosslyn Bay. It is possible therefore that wave setup may have contributed to elevated sea levels during this event.

At Darwin, a small relative peak of about 0.2 m around 22 February is associated with a burst of northwest monsoon winds (Figures 3e and 5e). At this time sea levels are also elevated to 0.5 m at Milner Bay (Figure 3d) by the northwesterly winds that are also directed into the Gulf of Carpentaria. At Hillarys, a sea level peak around 18 May is associated with a low pressure system off the southwest of the continent directing northwesterly flow onto the southwest coast. The final sequence of figures (Figures 4g-i) show the passage of a cold front that travels from west to east bringing southwesterly winds to the south coast of Australia and producing elevated sea levels in Esperance on 04 June (Figure 3g and 5g), Thevenard on 05 June (Figure 3h and 5h) and Portland and Burnie on 06 June (Figures 3i-j, 5i). Events of this type have been discussed in previous studies such as *McInnes and Hubbert*, [2003] and *McInnes et al.*[2009].

3.4 Tide-surge interaction

Understanding tide-surge interaction is important since it can alter timing, severity and intensity of storm surges [*Olbert et al.*, 2013; *Haigh et al.*, 2014b, *Antony and Unnikrishnan*, 2013]. In the context of the present study, a better understanding of the potential non-linear interaction between tides and surges contributes to an understanding of the uncertainty associated with the CMIP5-forced ocean model simulations. Due to computational constraints we demonstrate that the contribution of tides to the sea level can be neglected in the climate change projections.

Tide-surge interaction has been studied previously for parts of the Australian coast. In Bass Strait, the occurrence of strong westerly winds leads to a phase shift in the timing of the surge [*McInnes and Hubbert*, 2003; *Wijeratne et al.*, 2012]. On the northern shelf, the combination of strong tropical cyclone winds together with tides alters the amplitude of the water column [*Haigh et al.*, 2014b]. Both of these observed effects are in line with the notion of [*Rossiter*, 1961] that the interaction of tides and surges is one of mutual alteration. Simply put, depending on the size of the tide and the water depth the presence of tides alters the generation of the surge signal because the wind is more effective at creating a surge over lower sea levels. They conclude therefore that surges produced during low tide are generally larger [*Horsburgh and Wilson*, 2007] than those produced during high tides. Furthermore, since the tide and surge signals propagate as shallow water waves the presence of a surge increases the speed of the tidal wave so that the high tide arrives sooner than predicted. Therefore, when predicted tides are removed from tide gauge observations, the residuals can contain variations that are not driven by meteorological effects [e.g. *McInnes and Hubbert,* 2003].

Nat. Hazards Earth Syst. Sci. Discuss., https://doi.org/10.5194/nhess-2018-64
Manuscript under review for journal Nat. Hazards Earth Syst. Sci.
Discussion started: 26 March 2018

Natural Hazards and Earth System Sciences Discussions

To examine tide-surge interaction, sea level components (ζ) from the three baseline simulations are analysed (see Table 1). The first is forced by meteorology (B-M, i.e. atmospheric winds and pressure only) yielding surge only, ζ_M; the second (B-T) is forced by tides only, ζ_T; and the third (B-TM) combines tide and meteorological forcing, ζ_{TM}. Subtracting the ζ_T from the ζ_{TM} yields a time series of residuals ζ_R. By definition, differences between the time series of residuals and surges (i.e. ζ_R and ζ_M) are a result of tide-surge interaction.

The potential amplitude changes arising from tide-surge interactions around Australia are first examined by selecting the four-largest surges and residuals (separated by a 3-day window) per year from the 20-year ζ_M and ζ_R time series respectively and ranking the values. Although ranking of events removes the one-to-one relationship between the events in the surge and residual time series, it clarifies the relationship between the two. Not ranking the points (not shown) reveals a similar picture except that there is a larger degree of scatter of points especially for Broome, Darwin and Burnie indicating that at these locations a particular surge maximum may be larger or smaller than its residual counterpart. Figure 6 shows the relationship between the surges and residuals (red points and axes on top and right) are close to one, indicating that across the population of extremes the height of the surge is not systematically affected by the presence of tides. Exceptions are Broome, where the largest residuals (those greater than 0.6 m) are higher than the equivalent surges and Darwin and Burnie where residuals tend to be consistently higher than the surges by about 1-2cm.

To examine the effect of non-linear interaction on the timing of the surge maximum, we also examine the total water level at the time of the four largest annual maxima from the ζ_R and ζ_M. Here we add in the predicted tide height to the set of values at the times that the respective peaks occurred and again ranked the two groups and plotted their relationship (black points and bottom and left axes on Figure 6). In this case near one to one relationships are now only seen for eight of the fourteen stations. Tide-surge interaction is evident for Cape Ferguson, Rosslyn Bay, Broome, Darwin, Burnie and Stony Point. With the exception of Broome, the interaction is such that the total sea level at the times of the maximum ζ_R is smaller than the total sea level at times of maximum ζ_M. In other words when tides are included in the model simulations, the interaction between tides and surges causes the surges to occur during lower tides. The density distribution of the tides at the time of the 4-largest surges and residuals (not shown) indicates that the reason for the difference is that maximum residuals tend to occur on low waters for these locations. This 'phase locking' phenomenon occurs because the presence of a surge changes the speed of the tidal wave due to increased water depth and changes in the role of the bottom friction [e.g *Arns et al*., 2015]. As shown by *Horsburgh and Wilson* [2008] in observations, a first order effect of this is that the peak surge occurs before the maximum water level due to tides only.

From the above analysis we conclude that tide-surge interaction does exist, particularly over the shallow shelf areas in the northwest, northeast and Bass Strait where large tidal amplitudes enhance these interactions. The interactions in these locations affect both the timing and height of the surge. The effect on timing is particularly important for operational forecasting considerations. However, our analysis also shows that there is little overall difference in the magnitudes of the highest weather-driven events (i.e. ζ_R and ζ_M). This suggests that for the remainder of this study in which we are dealing with future changes in weather conditions and their effects on sea levels the omission of tidal forcing in the hydrodynamic simulations forced by climate models is not likely to alter the overall conclusions regarding changes to extreme sea levels [*Williams et al.,* 2016].

Nat. Hazards Earth Syst. Sci. Discuss., https://doi.org/10.5194/nhess-2018-64
Manuscript under review for journal Nat. Hazards Earth Syst. Sci.
Discussion started: 26 March 2018

Natural Hazards and Earth System Sciences Discussions

4 Climate change results

In this section, the primary focus is on changes in ESLs simulated by the climate change experiments listed in Table 2. First, quantile-quantile plots between the current climate (1980-1999) CC simulations and the B-M simulation are undertaken to examine the comparative performance of the different climate models under present climate conditions. Then the differences between the present and future climate conditions are examined.

4.1 Comparison with current climate

Figure 7 displays quantile-quantile sea level plots. They are used to compare the performance of the four CC experiments over the 1980-1999 period with those from the baseline (B-M) simulation. The figure suggests that the different climate models overall perform well in terms of generating a sea level response in the ocean model for the lower percentile ranges. The sea level response across the upper percentile range is on par with the baseline experiment for Spring Bay. Port Kembla, Cape Ferguson and Portland. Rosslyn Bay , Milner Bay, Brome, Thevenard, Port Stanvac and Stony Point display lower sea level responses here. For Darwin the lower percentiles are also overestimated by all models. Out of the four simulations CC-I performs the worst for Broome, Milner Bay, Thevenard and Port Stanvac. CC-H performs the best for Port Stanvac and Thevenard.

The average annual maximum sea levels from the B-M simulation are shown in Figure 8a together with values from the tide gauges residuals over 1980-1999. From Portland to Broome (counter clockwise), the B-M model is able to represent both magnitude and spatial variation in ESLs well. However at Hillarys on the west coast and Albany on the southwest coast the model underestimates the extremes. This underestimation may be partly due the contribution of wind-waves to ESLs (i.e. through wave setup), which is not considered in this study. A second, potentially larger contributor is sea level variably associated with baroclinic forcing and the Leeuwin Current [McInnes et al., 2016]. ESLs were also underestimated in this same region in the study of [*Haigh et al.*, 2014a], which, like this study, did not consider wave-driven or baroclinic processes influencing sea level. Model values are also underestimated at Port Stanvac and this may be due to poor model resolution of Gulf of St Vincent in which Port Stanvac is located.

Figure 8b shows the ensemble-average annual maximum sea levels of the four CC simulations. Results show that the climate model forcing leads to overall lower sea level extremes around the coastline of Australia compared to the baseline (B-M) simulation. This is likely to be at least partially due to the lower spatial and temporal resolution in the CC forcing (Table 1) compared to B-M. However, the variation in the ESL magnitude around the coastline is generally well captured with higher sea levels in the Gulf of Carpentaria and the southeastern coastline and Tasmania compared to the east and west coast regions.

We note that the skill of eight CMIP5 models in reproducing variables of surface temperature, precipitation and air pressure over continental areas by *Watterson et al*, [2014], including the four used here, led to model skill rankings which were markedly different to those determined by *Hemer and Trenham* [2015] in assessing global wind-wave climate skill using wind forcing from the same models. This highlights the need to assess the skill of the GCMs according to the task to which they are being used.

4.2 Seasonal mean maximum sea level change

To understand how seasonal changes in atmospheric forcing affect both the seasonal/ interannual and short-term (storm surge) sea level variations, the average of the largest sea level events per season over each set of 20 seasons is calculated and the 1980-1999 average values are subtracted from those of the 2080-2099 (Figure 9) for each of the CC simulations.

Nat. Hazards Earth Syst. Sci. Discuss., https://doi.org/10.5194/nhess-2018-64
Manuscript under review for journal Nat. Hazards Earth Syst. Sci.
Discussion started: 26 March 2018

Natural Hazards and Earth System Sciences Discussions

The largest positive anomalies of up to 0.1 m are seen in the Gulf of Carpentaria in DJF in the CC-A and CC-H simulations. The positive anomalies extend to MAM in CC-A, are also positive in CC-C but are negative by up to -0.1 m in CC-H. Along the southern mainland coastline, the changes are generally small and mostly negative consistent with results reported in *Colberg and McInnes* [2012]. However, positive changes are evident in CC-H in SON and CC-I in DJF and MAM over the southeast of the mainland and Tasmania. On the east and west coastal regions, the changes across models are typically small and within the range of ±0.04 m.

To better understand the atmospheric forcing changes responsible for these changes in sea level variability seen in the CC-A simulation between present and future time slices, the change in the seasonal mean and standard deviation (STD) of the wind speed is shown in Figure 10. Also shown on Figure 10a is the zero contour line of the zonal wind speed from 1980-1999 (blue) and 2080-2099 (red). This contour line identifies the delineation between the monsoon north-westerlies and tradewind easterlies over northern Australia during DJF and the subtropical ridge separating trade easterlies from mid-latitude westerlies over southern Australia throughout the year.

During DJF the eastward shift in the zero contour of the zonal wind in the 2080-2099 DJF is accompanied by a general increase in wind speed across tropical Australia and wind STD within the Gulf of Carpentaria. This suggests there is a greater influence of northeast monsoon winds on the Gulf of Carpentaria, which provide favourable conditions for increased sea levels in the Gulf [*Oliver and Thompson*, 2008]. The CC-H simulations produce a similar increase in sea levels in the Gulf during DJF, also related to northwest monsoon winds penetrating further east and increased variability in this region. The reasons for the positive anomalies in the ACCESS1.0 and the CC-C simulations in MAM are less clear since both simulations show a decrease in mean winds and variability in the Gulf of Carpentaria (not shown).

Along the southern coastline of the continent and Tasmania there is a tendency for a decrease in ESLs in most seasons of the models. As illustrated in figure 10 for CC-A, this is related to the southward movement of the subtropical ridge, reduced wind variability and the greater frequency of non-storm surge producing easterly winds. In CC-H in SON, positive anomalies in sea level are seen and this is related to both an increase in westerlies over Tasmania and a strong increase in STD (not shown). The weak increase in CC-I in DJF is related to the minimal southward movement of the mid-latitude storm belt together with an increase in the STD in that model.

The overall projected changes to maximum ESL events around Australia are summarised in Figure 11. These ensemble differences are generated by finding the difference between the maximum sea level for 1990-1999 and 2080-2099 time periods for each of the CC ensembles members. Since each time period is 20 years, this equates to the (empirical) change in 1 in 20 year average recurrence interval; the minimum, average and maximum of these ensemble differences are shown in the upper, middle and lower subplot of Figure 11 and give an indication of uncertainty. The minimum changes are negative around the entire coastline indicating an average decrease in the approximate 20-year average recurrence interval in the range of 0 to 0.2 m. The largest projected decreases are on the eastern side of the Gulf of Carpentaria, the central west and south coasts. The average change across the four models is weakly negative around most of the coastline with weak positive anomalies evident along the northern and northwest shelf. The ensemble maximum changes show weak positive anomalies of up to 0.04 m along the southeast and east coast. The largest positive changes of up to 0.2 m occur on the eastern side of the Gulf of Carpentaria, the central north coast and parts of the northwest and west coast. Negative anomalies occur on the central south and southwest coasts.

Nat. Hazards Earth Syst. Sci. Discuss., https://doi.org/10.5194/nhess-2018-64
Manuscript under review for journal Nat. Hazards Earth Syst. Sci.
Discussion started: 26 March 2018

Natural Hazards and Earth System Sciences Discussions

5 Summary and Concluding Discussion

In order to investigate characteristics of extreme sea levels (ESLs), a depth-averaged hydrodynamic model covering Australia was implemented at 5 km spatial resolution and baseline simulations carried out over the period 1981 to 2012 with hourly atmospheric and tidal forcing. Overall, simulations of longer-term (seasonal and interannual) and short-term (weather-driven) variations in sea level compare well with those measured at tide gauges, with differences largely reflecting the absence of baroclinic forcing in the model. The modelled tides agree well with observations in all except the Gulf of Carpentaria where the O1 and K1 constituents were underestimated by the model and the southwestern coast where the M2 and S2 constituents were underestimated. The effect of tide-surge interaction on the amplitude of the meteorological component of sea level extremes (e.g. storm surge) was found to be small for much of the coastline; the main effect of the interaction being on the timing of the peak sea levels rather than the annual maximum sea levels. This suggested that in climate model-forced hydrodynamic simulations that assess how atmospheric circulation changes affect ESLs, tidal forcing can be neglected. This is further supported by the finding (across a large number of north Atlantic tide gauges) that while tide-surge interaction may affect the timing of maximum water levels, tides have no direct effect on the magnitude of storm surge [*Williams et al.,* 2016].

Hydrodynamic simulations were carried out over the periods 1980-1999 and 2080-2099 using forcing from four CMIP5 climate models run with the RCP 8.5 emission scenario. Changes in ESLs were generally small and mostly negative along much of the coastline. However, in some areas ESL changes were sensitive to the movement of major atmospheric circulation patterns. This was because of factors such as bathymetric depths and coastline orientation in relation to the weather forcing that favoured the occurrence of certain sea level extremes. For example, the Gulf of Carpentaria exhibited relatively large increases in ESLs in the climate models that simulated eastward movement of the northwest monsoon during the DJF season. However, since only two of the four climate model simulations simulated this change in the future climate, the finding is uncertain. Along the mainland south coast, there was a greater tendency for the models to indicate a reduction of ESLs in the future, particularly during winter which is also consistent with the finding of *Colberg and McInnes* [2012] using CMIP3 and regional climate models for the atmospheric forcing.

With regards to the projected ESL changes, we note several caveats. First, the changes are subject to large uncertainty due to the small number of CMIP5 models used to force the hydrodynamic model. Furthermore, certain important drivers of ESLs are poorly represented in climate models in general (e.g. tropical cyclones). Future studies may address these uncertainties by considering a larger ensemble of hydrodynamic simulations forced with higher resolution climate models that better capture important small scale meteorological features, or by perturbing characteristics of historical storms to produce plausible future synthetic storm libraries [*McInnes et al.*, 2014]. We also note that wind-waves also contribute to sea level extremes and these effects and their potential changes need to be assessed for a more complete understanding of the changes to sea level extremes [*e.g. Hoeke et al.*, 2015]. The increasing availability of wave climate change assessments [e.g. *Hemer et al.*, 2013; *Hemer and Trenham*, 2015] will facilitate future efforts in this regard. Also, while previous studies similar to this one have focused on changes to ESLs and coastal inundation [e.g. *Colberg and McInnes*, 2012;. *McInnes et al.*, 2013], consideration of changes to other variables, including currents is emerging [e.g. *Lowe et al.*, 2009]. Changes to wind-driven coastal currents, which could be considered using the modelling framework presented in this study (but is beyond the scope of this paper), is also potentially important in the context of coastal erosion and shoreline change [*Gornitz*, 1991; *O'Grady et al.*, 2015].

Nat. Hazards Earth Syst. Sci. Discuss., https://doi.org/10.5194/nhess-2018-64
Manuscript under review for journal Nat. Hazards Earth Syst. Sci.
Discussion started: 26 March 2018

6 References

Antony, C., and A. Unnikrishnan (2013), Observed characteristics of tide-surge interaction along the east coast of India and the head of Bay of Bengal, Estuarine, Coastal and Shelf Science, 131, 6-11.

Arns, A., Wahl, T., Dangendorf, S., & Jensen, J. (2015). The impact of sea level rise on storm surge water levels in the northern part of the German Bight. Coastal Engineering, 96, 118–131.

Chapman, D. C. (1985), Numerical Treatment of Cross-Shelf Open Boundaries in a Barotropic Coastal Ocean Model, Journal of physical oceanography, 15(8), 1060-1075.

Colberg, F., and K. L. McInnes (2012), The impact of future changes in weather patterns on extreme sea levels over southern Australia, Journal of Geophysical Research: Oceans, 117(C8), C08001.

Flather, R. A. (1976), A tidal model of the north-west European continental shelf., Memoires de la societe Royale des Sciences de Liege, 10, 141-164.

Forbes, A., and J. Church (1983), Circulation in the Gulf of Carpentaria. II. Residual currents and mean sea level, Marine and Freshwater Research, 34(1), 11-22.

Godfrey, J., and K. Ridgway (1985), The large-scale environment of the poleward-flowing Leeuwin Current, Western Australia: longshore steric height gradients, wind stresses and geostrophic flow, Journal of physical oceanography, 15(5), 481-495.

Gordon, H., S. O'Farrell, M. Collier, M. Dix, L. Rotstayn, E. Kowalczyk, T. Hirst, and I. Watterson (2010), The CSIRO Mk3. 5 climate model, CAWCR.

Gornitz, V. (1991), Global coastal hazards from future sea level rise, Palaeogeography, Palaeoclimatology, Palaeoecology, 89(4), 379-398.

Green, D., L. Alexander, K. L. McInnes, J. Church, N. Nicholls, and W. N. (2010), An assessment of climate change impacts and adaptation for the Torres Strait Islands, Climatic Change, 102, 405–433.

Egbert, G. D., A. F. Bennett, and M. G. Foreman (1994), TOPEX/POSEIDON tides estimated using a global inverse model, Journal of Geophysical Research: Oceans (1978–2012), 99(C12), 24821-24852.

Egbert, G. D., and S. Y. Erofeeva (2002), Efficient inverse modeling of barotropic ocean tides, Journal of Atmospheric & Oceanic Technology, 19(2).

Haigh, I., E. M. S. Wijeratne, L. MacPherson, C. Pattiaratchi, M. Mason, R. Crompton, and S. George (2014a), Estimating present day extreme water level exceedance probabilities around the coastline of Australia: tides, extra-tropical storm surges and mean sea level, Clim Dyn, 42, 121-138.

Haigh, I., L. MacPherson, M. Mason, E. M. S. Wijeratne, C. Pattiaratchi, R. Crompton, and S. George (2014b), Estimating present day extreme water level exceedance probabilities around the coastline of Australia: tropical cyclone-induced storm surges, Clim Dyn, 42, 139-147.

Hanson, S., R. Nicholls, N. Ranger, S. Hallegatte, J. Corfee-Morlot, C. Herweijer, and J. Chateau (2011), A global ranking of port cities with high exposure to climate extremes, Climatic Change, 104(1), 89-111.

Hunter, J. R., Church, J. A., White, N. J., & Zhang, X. (2013). Towards a global regionally varying allowance for sea-level rise. Ocean Engineering, 71, 17–27. https://doi.org/10.1016/j.oceaneng.2012.12.041

Hemer, M. A., Y. Fan, N. Mori, A. Semedo, and X. L. Wang (2013), Projected changes in wave climate from a multi-model ensemble, Nature Clim. Change, advance online publication.

Hemer, M. A., & Trenham, C. E. (2016). Evaluation of a CMIP5 derived dynamical global wind wave climate model ensemble. Ocean Modelling, 103, 190–203. https://doi.org/10.1016/J.OCEMOD.2015.10.009

Hoeke, R., McInnes, K., & O'Grady, J. (2015). Wind and Wave Setup Contributions to Extreme Sea Levels at a Tropical High Island: A Stochastic Cyclone Simulation Study for Apia, Samoa. Journal of Marine Science and Engineering, 3(3), 1117–1135. https://doi.org/10.3390/jmse3031117

Horsburgh, K., and C. Wilson (2007), Tide-surge interaction and its role in the distribution of surge residuals in the North Sea, Journal of Geophysical Research: Oceans (1978–2012), 112(C8).

Jordà, G., D. Gomis, E. Álvarez-Fanjul, and S. Somot (2012), Atmospheric contribution to Mediterranean and nearby Atlantic sea level variability under different climate change scenarios, Global and Planetary Change, 80–81(0), 198-214.

Jakobsson, M., R. Macnab, M. Mayer, R. Anderson, M. Edwards, J. Hatzky, H-W. Schenke, and P. Johnson (2008) , An improved bathymetric portrayal of the Arctic Ocean: Implications for ocean modeling and geological, geophysical and oceanographic analyses, v. 35, L07602, Geophysical Research Letters, doi:10.1029/2008GL033520

Jungclaus, J. H., N. Keenlyside, M. Botzet, H. Haak, J. J. Luo, M. Latif, J. Marotzke, U. Mikolajewicz, and E. Roeckner (2006), Ocean Circulation and Tropical Variability in the Coupled Model ECHAM5/MPI-OM, Journal of Climate, 19(16), 3952-3972.

Kistler, R., et al. (2001), The NCEP–NCAR 50–Year Reanalysis: Monthly Means CD–ROM and Documentation, Bulletin of the American Meteorological Society, 82(2), 247-267.

Kumar, R. K., A. K. Sahai, K. K. Kumar, S. K. Patwardhan, P. K. Mishra, J. V. Revadekar, K. Kamala, and G. B. Pant (2006), High-resolution climate change scenarios for India for the 21st century, Current Science, 90 (3), 334-345.

Lin, N., K. Emanuel, M. Oppenheimer, and E. Vanmarcke (2012), Physically based assessment of hurricane surge threat under climate change, Nature Clim. Change, 2(6), 462-467.

Lowe, J. A., et al. (2009), UK Climate Projections science report: Marine and coastal projections., edited, p. 96 pp, Met Office Hadley Centre, Exeter, UK.

Marcos, M., G. Jordà, D. Gomis, and B. Pérez (2011), Changes in storm surges in southern Europe from a regional model under climate change scenarios, Global and Planetary Change, 77(3–4), 116-128.

McGregor, J. L., and M. R. Dix (2008), An updated description of the conformal-cubic atmospheric model, in High resolution numerical modelling of the atmosphere and ocean, edited, pp. 51-75, Springer.

McInnes, K. L., and G. D. Hubbert (2001), The impact of eastern Australian cut-off lows on coastal sea levels, Meteorological Applications, 8(2), 229-243.

McInnes, K. L., and G. D. Hubbert (2003), A numerical modelling study of storm surges in Bass Strait, Australian meteorological magazine 52 143-156

McInnes, K. L., Macadam, I., Hubbert, G.D. and O'Grady, J.G. (2009), A Modelling Approach for Estimating the Frequency of Sea Level Extremes and the Impact of Climate Change in Southeast Australia. , Natural Hazards 51, 115–137.

McInnes, K. L., T. A. Erwin, and J. M. Bathols (2011), Global Climate Model projected changes in 10 m wind speed and direction due to anthropogenic climate change, Atmospheric Science Letters, 12(4), 325-333.

McInnes, K. L., et al. (2012), Climate Futures for Tasmania: Extreme tide and sea-level eventsRep., 40 pp pp, Antarctic Climate and Ecosystems CRC.

McInnes, K. L., I. Macadam, G. Hubbert, and J. O'Grady (2013), An assessment of current and future vulnerability to coastal inundation due to sea-level extremes in Victoria, southeast Australia, International Journal of Climatology, 33(1), 33-47.

Nat. Hazards Earth Syst. Sci. Discuss., https://doi.org/10.5194/nhess-2018-64
Manuscript under review for journal Nat. Hazards Earth Syst. Sci.
Discussion started: 26 March 2018

Natural Hazards and Earth System Sciences Discussions

McInnes, K. L., K. J. E. Walsh, R. K. Hoeke, J. G. O'Grady, F. Colberg, and G. D. Hubbert (2014), Quantifying storm tide risk in Fiji due to climate variability and change, Global and Planetary Change, 116, 115–129.

McInnes, K. L., J. A. Church, D. Monselesan, J. R. Hunter, J. G. O'Grady, Haigh I. D., and X. Zhang (2015), Sea-level Rise Projections for Australia: Information for Impact and Adaptation Planning, Australian Meteorological and Oceanographic Journal, submitted.

McInnes, K.L., White, C.J., Haigh, I.D., Hemer, M.A., Hoeke, R.K., Holbrook, N.J., Kiem, A.S., Oliver, E.C.J., Ranasinghe, R., Walsh, K.J.E., Westra, S. and Cox, R.2016: Natural hazards in Australia: sea level and coastal extremes. Climatic Change. DOI: 10.1007/s10584-016-1647-8

Menéndez, M., and P. L. Woodworth (2010), Changes in extreme high water levels based on a quasi-global tide-gauge data set, Journal of Geophysical Research: Oceans, 115(C10), C10011.

Murphy, J. M., B. B. B. Booth, M. Collins, G. R. Harris, D. M. H. Sexton, and M. J. Webb (2007), A methodology for probabilistic predictions of regional climate change from perturbed physics ensembles, Philosophical Transactions of the Royal Society A: Mathematical, Physical and Engineering Sciences, 365(1857), 1993-2028.

Nakićenović, N., and R. Swart (2000), Emission scenariosRep., 20 pp pp, Intergovernmental Panel for Climate Change

Nicholls, R. J., N. Marinova, J. A. Lowe, S. Brown, P. Vellinga, D. De Gusmao, J. Hinkel, and R. S. Tol (2011), Sea-level rise and its possible impacts given a 'beyond 4 C world'in the twenty-first century, Philosophical Transactions of the Royal Society A: Mathematical, Physical and Engineering Sciences, 369(1934), 161-181.

O'Grady, J. G., K. L. McInnes, F. Colberg, M. A. Hemer, and A. V. Babanin (2015), Longshore wind, waves and currents: climate and climate projections at Ninety Mile Beach, southeastern Australia, International Journal of Climatology, n/a-n/a.

Olbert, A., S. Nash, C. Cunnane, and M. Hartnett (2013), Tide–surge interactions and their effects on total sea levels in Irish coastal waters, Ocean Dynamics, 63(6), 599-614.

Oliver, E. C. J., and K. R. Thompson (2011), Sea level and circulation variability of the Gulf of Carpentaria: Influence of the Madden-Julian Oscillation and the adjacent deep ocean, Journal of Geophysical Research: Oceans, 116(C2), C02019.

Pattiaratchi, C. B., and M. Eliot (2008), Sea level variability in southwest Australia: from hours to decades., in Proceedings of the 31st ASCE international conference on coastal engineering, edited, Hamburg.

Pawlowicz, R., B. Beardsley, and S. Lentz (2002), Classical tidal harmonic analysis including error estimates in MATLAB using T_TIDE, Computers & Geosciences, 28(8), 929-937.

Pickering, M. D., K. J. Horsburgh, J. R. Blundell, J. J. M. Hirschi, R. J. Nicholls, M. Verlaan, and N. C. Wells, 2017: The impact of future sea-level rise on the global tides. Continental Shelf Research, 142, 50-68

Rossiter, J. R. (1961), Interaction Between Tide and Surge in the Thames, Geophys J Int, 6(1), 29-53.

Saha, S., et al. (2010), The NCEP Climate Forecast System Reanalysis, Bulletin of the American Meteorological Society, 91(8), 1015-1057.

Shchepetkin, A. F., and J. C. McWilliams (2005), The regional oceanic modeling system (ROMS): a split-explicit, free-surface, topography-following-coordinate oceanic model, Ocean Modelling, 9(4), 347-404.

Sterl, A., H. van den Brink, H. de Vries, R. Haarsma, and E. van Meijgaard (2009), An ensemble study of extreme storm surge related water levels in the North Sea in a changing climate, Ocean Science, 5(3), 369-378.

Taylor, K. E., R. J. Stouffer, and G. A. Meehl (2012), An Overview of CMIP5 and the Experiment Design, Bulletin of the American Meteorological Society, 93(4), 485-498.

Tregoning, P., K. Lambeck, and G. Ramillien (2008), GRACE estimates of sea surface height anomalies in the Gulf of Carpentaria, Australia, Earth and Planetary Science Letters, 271(1), 241-244.

Trenham, C. E., M. A. Hemer, T. H. Durrant, and D. J. M. Greenslade (2013), PACCSAP Wind-wave Climate: High resolution windwave climate and projections of change in the Pacific region for coastal hazard assessmentsRep., 44 pp.

Unnikrishnan, A., M. RameshKumar, and B. Sindhu (2011), Tropical cyclones in the Bay of Bengal and extreme sea-level projections along the east coast of India in a future climate scenario, Current Science, 101(3), 327-331.

Wahl, T., Haigh, I. D., Nicholls, R. J., Arns, A., Dangendorf, S., Hinkel, J., & Slangen, A. B. A. (2017). Understanding extreme sea levels for broad-scale coastal impact and adaptation analysis. Nature Communications, 8, 16075. https://doi.org/10.1038/ncomms16075

Williams, J., Horsburgh, K. J., Williams, J. A., & Proctor, R. N. F. (2016). Tide and skew surge independence: New insights for flood risk. Geophysical Research Letters, 43(12), 6410–6417. https://doi.org/10.1002/2016GL069522\

Wijeratne, E. M. S., C. B. Pattiaratchi, M. Eliot, and I. D. Haigh (2012), Tidal characteristics in Bass Strait, south-east Australia, Estuarine, Coastal and Shelf Science, 114(0), 156-165.

Yasuda, T., S. Nakajo, S. Kim, H. Mase, N. Mori, and K. Horsburgh (2014), Evaluation of future storm surge risk in East Asia based on state-of-the-art climate change projection, Coastal Engineering, 83(0), 65-71.

Nat. Hazards Earth Syst. Sci. Discuss., https://doi.org/10.5194/nhess-2018-64
Manuscript under review for journal Nat. Hazards Earth Syst. Sci.
Discussion started: 26 March 2018

Natural Hazards and Earth System Sciences Discussions

Table 1: Summary of model experiments carried out. The spatial and temporal resolution refer to the source of the atmospheric forcing applied to the ROMS model.

	ROMS Model Experiments	Time Period		Atmospheric Forcing	Emission Scenario	Spatial Resolution (° lat × °long)	Temporal Resolution (hours)	Tide
		Historical	Future					
	Baseline							
B-TM	Tide+Meteorology	1981 - 2012		CFSR		0.3° × 0.3°	Hourly	Yes
B-T	Tide Only	1981 - 2012		None				Yes
B-M	Meteorology Only	1981 - 2012		CFSR		0.3° × 0.3°	Hourly	No
	Climate Change							
CC-A	ACCESS1.0	1980 - 1999	2080 - 2099	ACCESS1.0	RCP 8.5	1.9°×1.2°	3-hourly	No
CC-H	HadGEM-ES	1980 - 1999	2080 - 2099	HadGEM-ES	RCP 8.5	1.9°×1.2°	3-hourly	No
CC-I	INMCM4	1980 - 1999	2080 - 2099	INMCM4	RCP 8.5	2.0°×1.5°	3-hourly	No
CC-C	CNRM-CM5	1980 - 1999	2080 - 2099	CNRM-CM5	RCP 8.5	1.4°×1.4°	3-hourly	No

Table 2: Root mean square errors (RMSE), mean standard deviation errors (STDE) and correlation coefficients for the astronomical tide, residual, seasonal signal and total water levels for the period 1993 to 2012 (except for Port Stanvac which is over the period 1993-2009). For sites marked with (*) a 24-hour running mean was applied to both the de-tided observations and model simulations to remove noise arising from the de-tiding process that was most pronounced at these locations.

Site Name	RMSE				STDE				Correlation			
	Season.	Tide	Resid.	Total	Season.	Tide	Resid.	Total	Season.	Tide	Resid.	Total
Spring Bay	0.04	0.07	0.06	0.11	-0.01	0.06	0.00	0.05	0.62	0.99	0.85	0.95
Port Kembla	0.05	0.05	0.06	0.13	-0.03	0.03	-0.02	0.03	0.39	0.99	0.56	0.95
Rosslyn Bay*	0.06	0.26	0.05	0.34	-0.05	-0.20	-0.03	-0.20	0.75	0.99	0.70	0.96
Cape Ferguson*	0.07	0.17	0.06	0.25	-0.06	0.10	-0.05	0.09	0.77	0.98	0.73	0.95
Milner Bay	0.15	0.15	0.11	0.23	-0.14	-0.09	-0.08	-0.15	0.91	0.90	0.78	0.85
Darwin*	0.10	0.30	0.06	0.42	-0.09	-0.02	-0.04	-0.03	0.73	0.98	0.55	0.97
Broome*	0.08	0.40	0.07	0.63	-0.07	-0.08	-0.03	-0.07	0.74	0.98	0.39	0.95
Hillarys	0.10	0.04	0.08	0.13	-0.08	-0.01	-0.06	-0.06	0.53	0.97	0.80	0.84
Esperance	0.07	0.08	0.08	0.13	-0.05	-0.03	-0.04	-0.06	0.57	0.93	0.81	0.87
Thevenard	0.07	0.21	0.11	0.25	-0.04	-0.12	-0.06	-0.14	0.62	0.87	0.84	0.85
Port Stanvac	0.07	0.37	0.10	0.39	-0.04	-0.19	-0.06	-0.20	0.75	0.67	0.88	0.70
Portland	0.06	0.06	0.06	0.10	-0.03	-0.01	-0.02	-0.02	0.66	0.96	0.86	0.92
Stony Point	0.05	0.15	0.07	0.20	-0.02	-0.07	-0.03	-0.08	0.66	0.98	0.84	0.96
Burnie	0.05	0.13	0.06	0.25	-0.01	-0.02	-0.02	-0.02	0.43	0.99	0.77	0.96
Average	0.07	0.17	0.07	0.25	-0.05	-0.05	-0.04	-0.06	0.65	0.94	0.74	0.91

Nat. Hazards Earth Syst. Sci. Discuss., https://doi.org/10.5194/nhess-2018-64
Manuscript under review for journal Nat. Hazards Earth Syst. Sci.
Discussion started: 26 March 2018

Natural Hazards and Earth System Sciences
Discussions

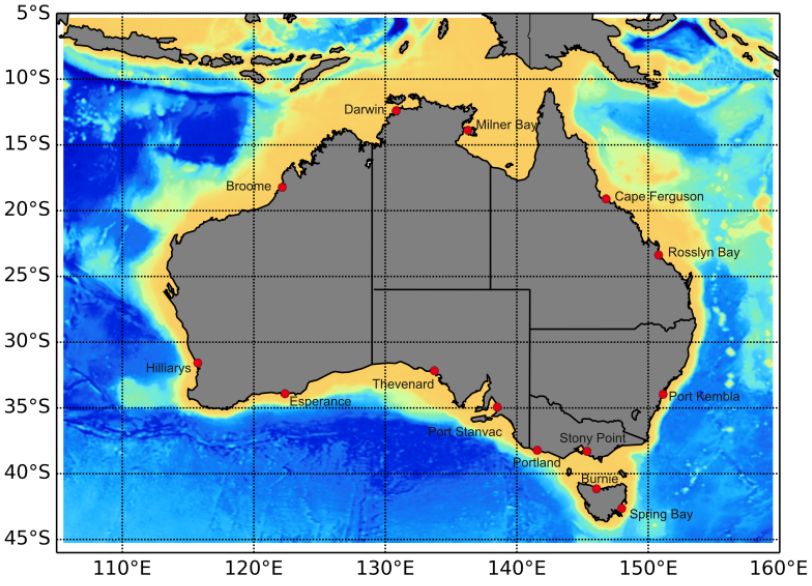

Figure 1: The region covered by the hydrodynamic model. Red dots mark the locations of the tide gauges used for validation of baseline simulations listed in Table 2.

5

Nat. Hazards Earth Syst. Sci. Discuss., https://doi.org/10.5194/nhess-2018-64
Manuscript under review for journal Nat. Hazards Earth Syst. Sci.
Discussion started: 26 March 2018

Natural Hazards and Earth System Sciences
Discussions

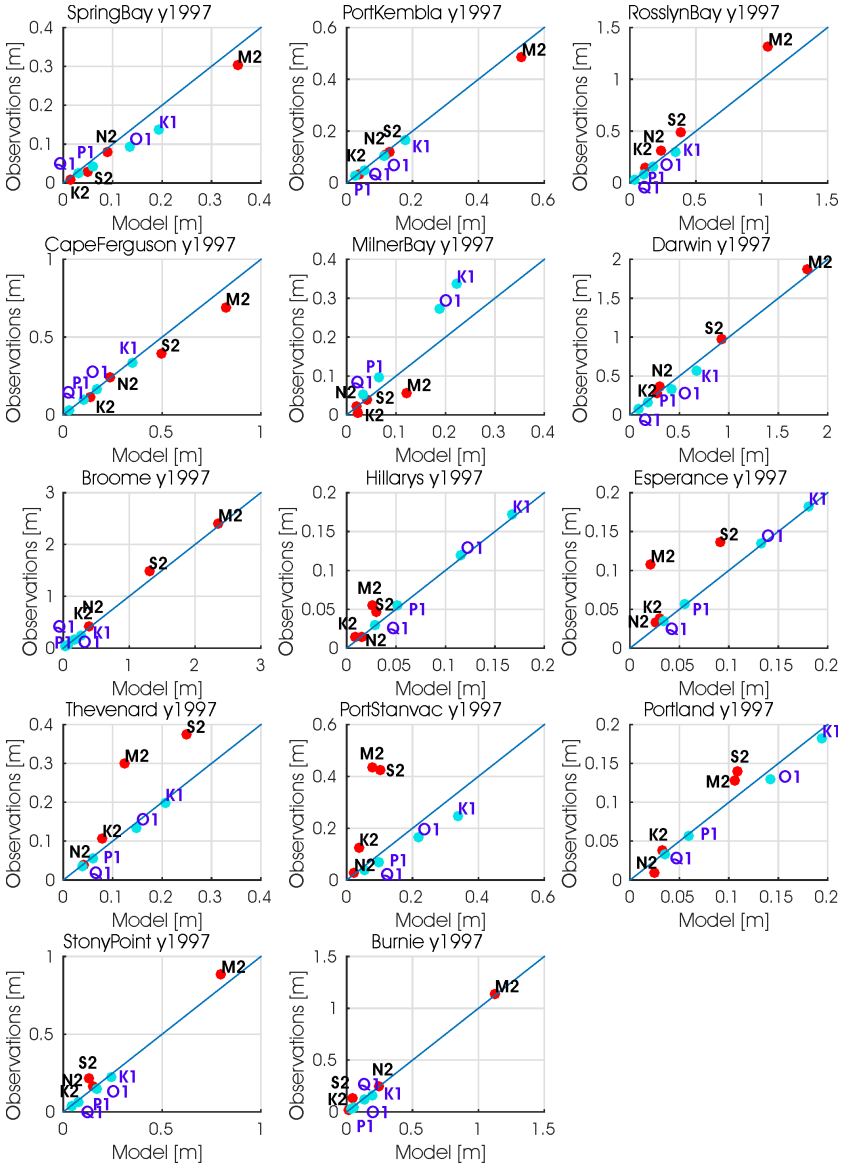

Figure 2: Comparison between tide constituents estimated from observations and modelled for the tide gauge locations shown in Figure 1.

Nat. Hazards Earth Syst. Sci. Discuss., https://doi.org/10.5194/nhess-2018-64
Manuscript under review for journal Nat. Hazards Earth Syst. Sci.
Discussion started: 26 March 2018

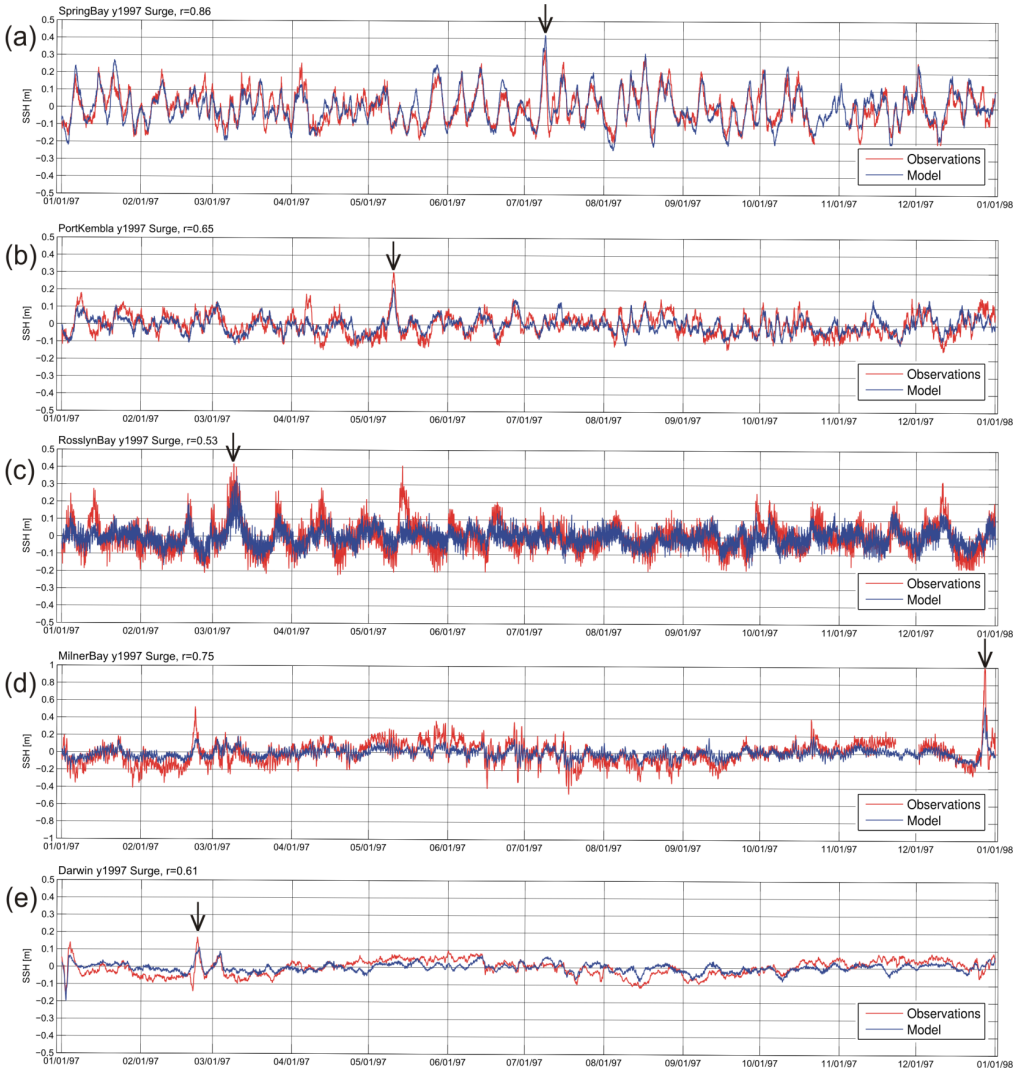

Figure 3: Comparison of sea level residuals from tide gauge observations (red) and baseline model experiment (B-TM) for 1997. Black arrows indicate storm surge events discussed in the text.

Nat. Hazards Earth Syst. Sci. Discuss., https://doi.org/10.5194/nhess-2018-64
Manuscript under review for journal Nat. Hazards Earth Syst. Sci.
Discussion started: 26 March 2018

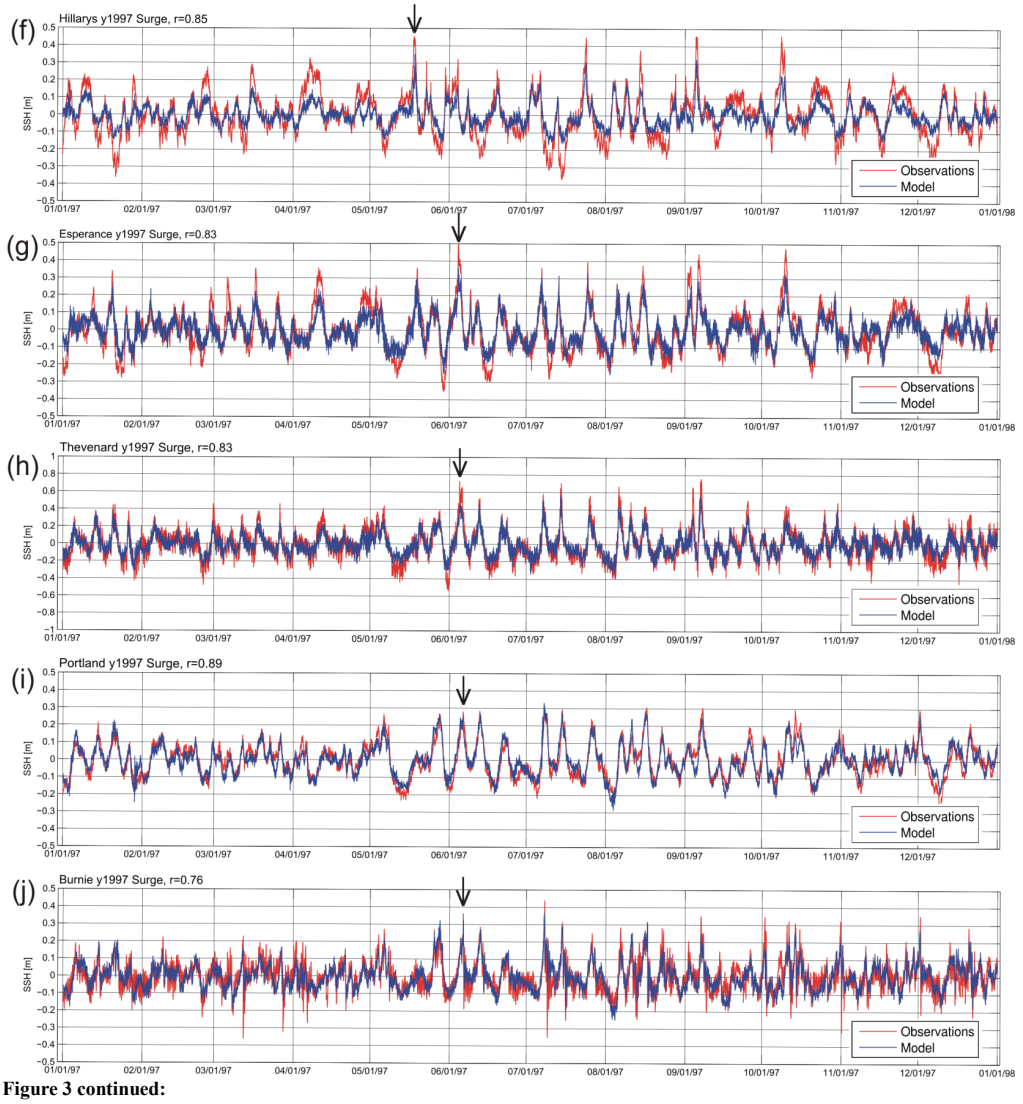

Figure 3 continued:

5

Nat. Hazards Earth Syst. Sci. Discuss., https://doi.org/10.5194/nhess-2018-64
Manuscript under review for journal Nat. Hazards Earth Syst. Sci.
Discussion started: 26 March 2018

Natural Hazards and Earth System Sciences
Discussions

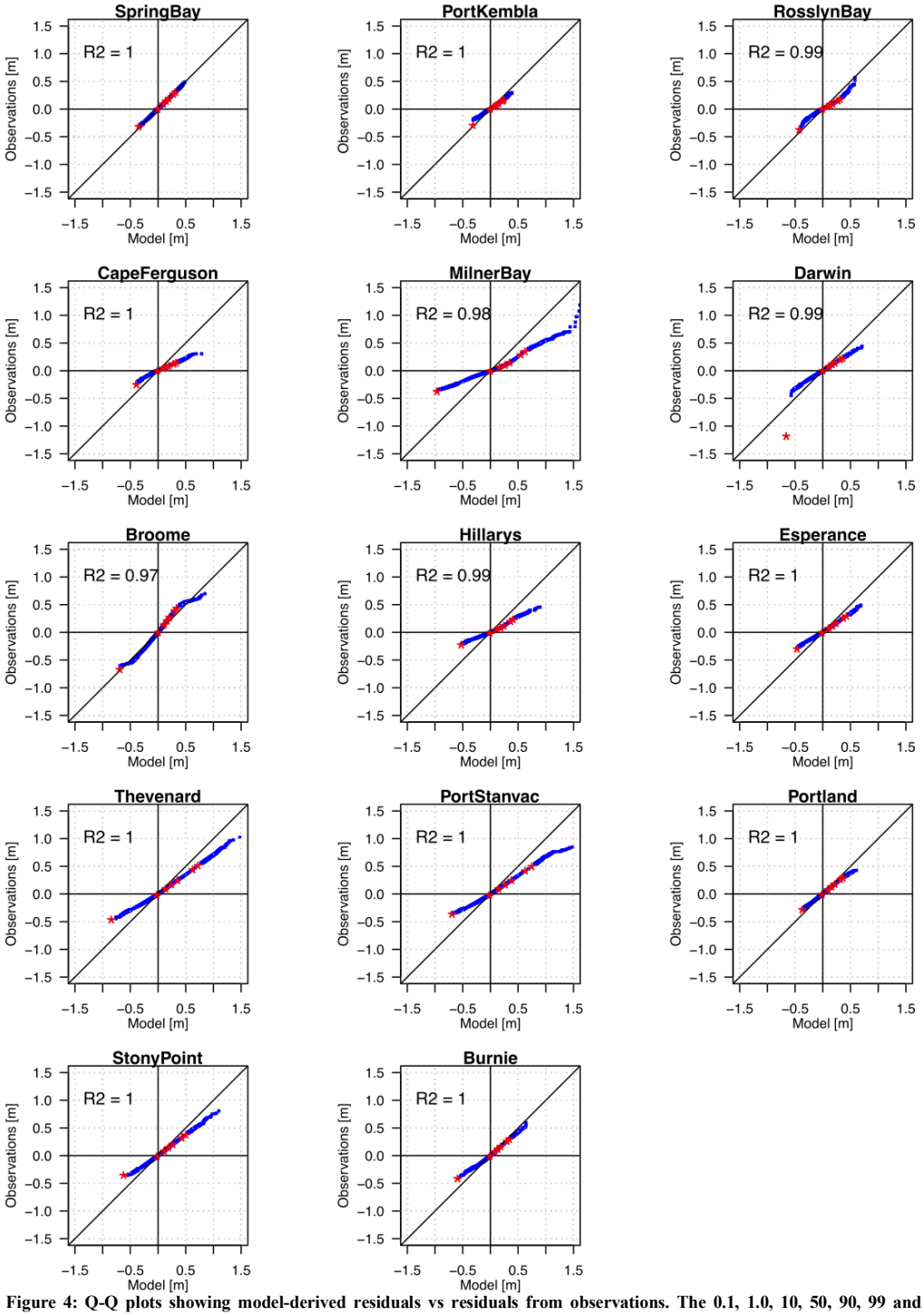

Figure 4: Q-Q plots showing model-derived residuals vs residuals from observations. The 0.1, 1.0, 10, 50, 90, 99 and 99.9 percentiles are highlighted in red.

Nat. Hazards Earth Syst. Sci. Discuss., https://doi.org/10.5194/nhess-2018-64
Manuscript under review for journal Nat. Hazards Earth Syst. Sci.
Discussion started: 26 March 2018

Natural Hazards and Earth System Sciences
Discussions

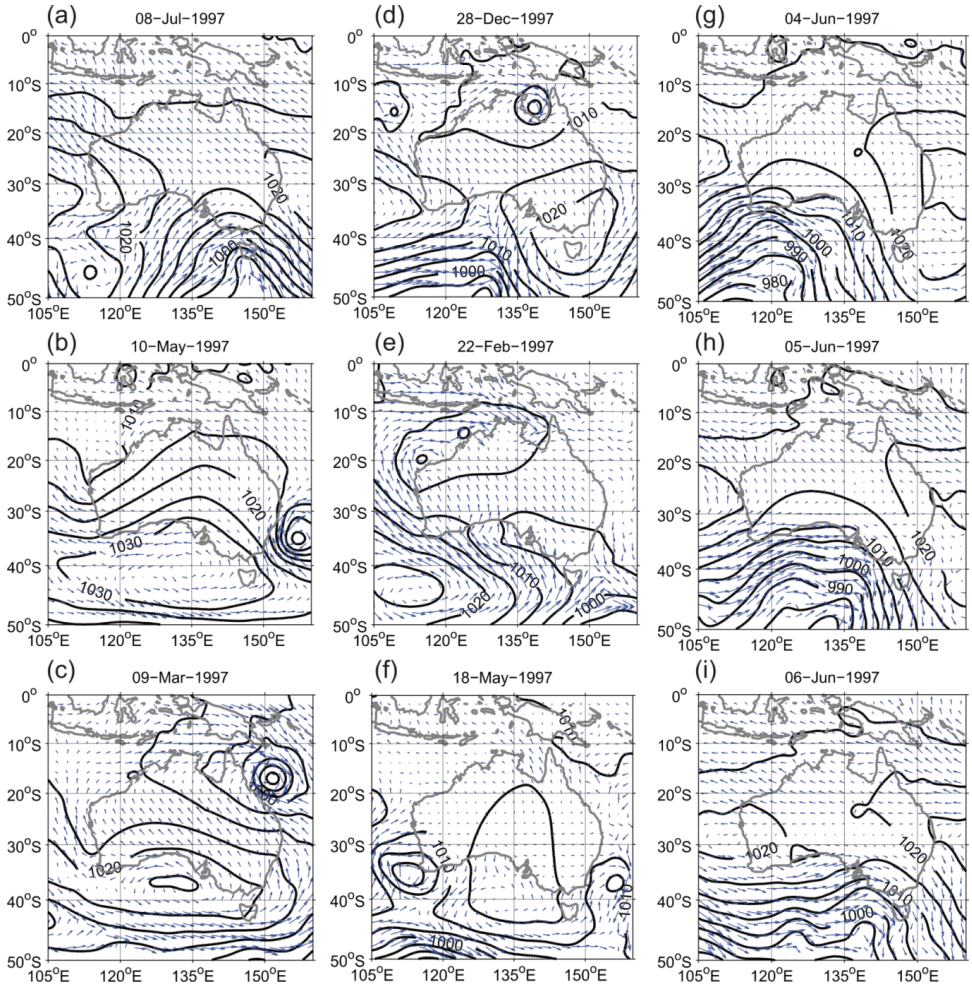

Figure 5: Mean sea level pressure and surface winds from CFSR reanalyses for the events indicated with black arrows in Figure 3. Note, Figure 3i, j both relate to the same synoptic pattern of Figure 5i.

Nat. Hazards Earth Syst. Sci. Discuss., https://doi.org/10.5194/nhess-2018-64
Manuscript under review for journal Nat. Hazards Earth Syst. Sci.
Discussion started: 26 March 2018

Natural Hazards and Earth System Sciences
Discussions

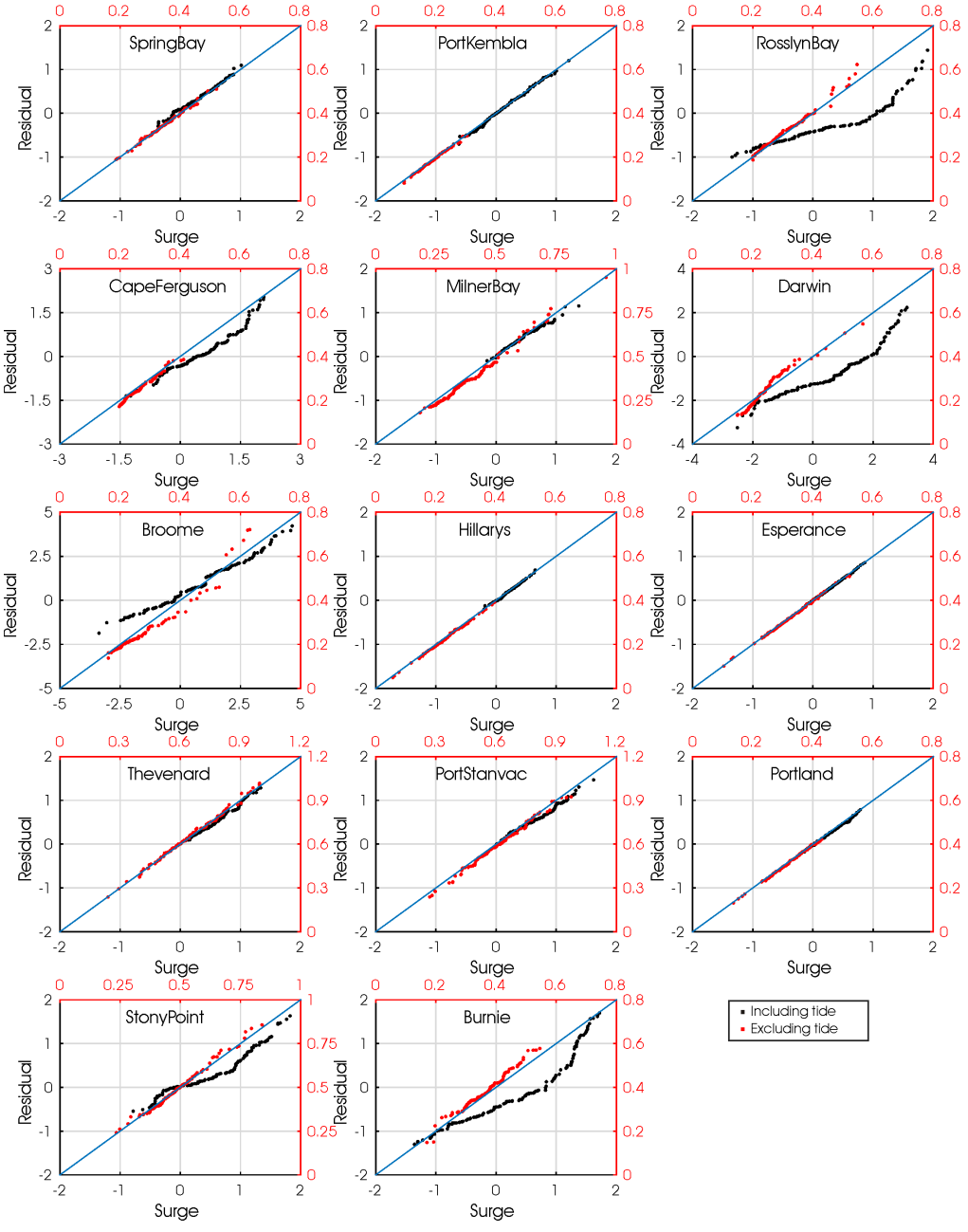

Figure 6: Comparison between modelled surges and residuals including tides (black), excluding tides (red) for each location (see text for details).

Nat. Hazards Earth Syst. Sci. Discuss., https://doi.org/10.5194/nhess-2018-64
Manuscript under review for journal Nat. Hazards Earth Syst. Sci.
Discussion started: 26 March 2018

Natural Hazards and Earth System Sciences
Discussions

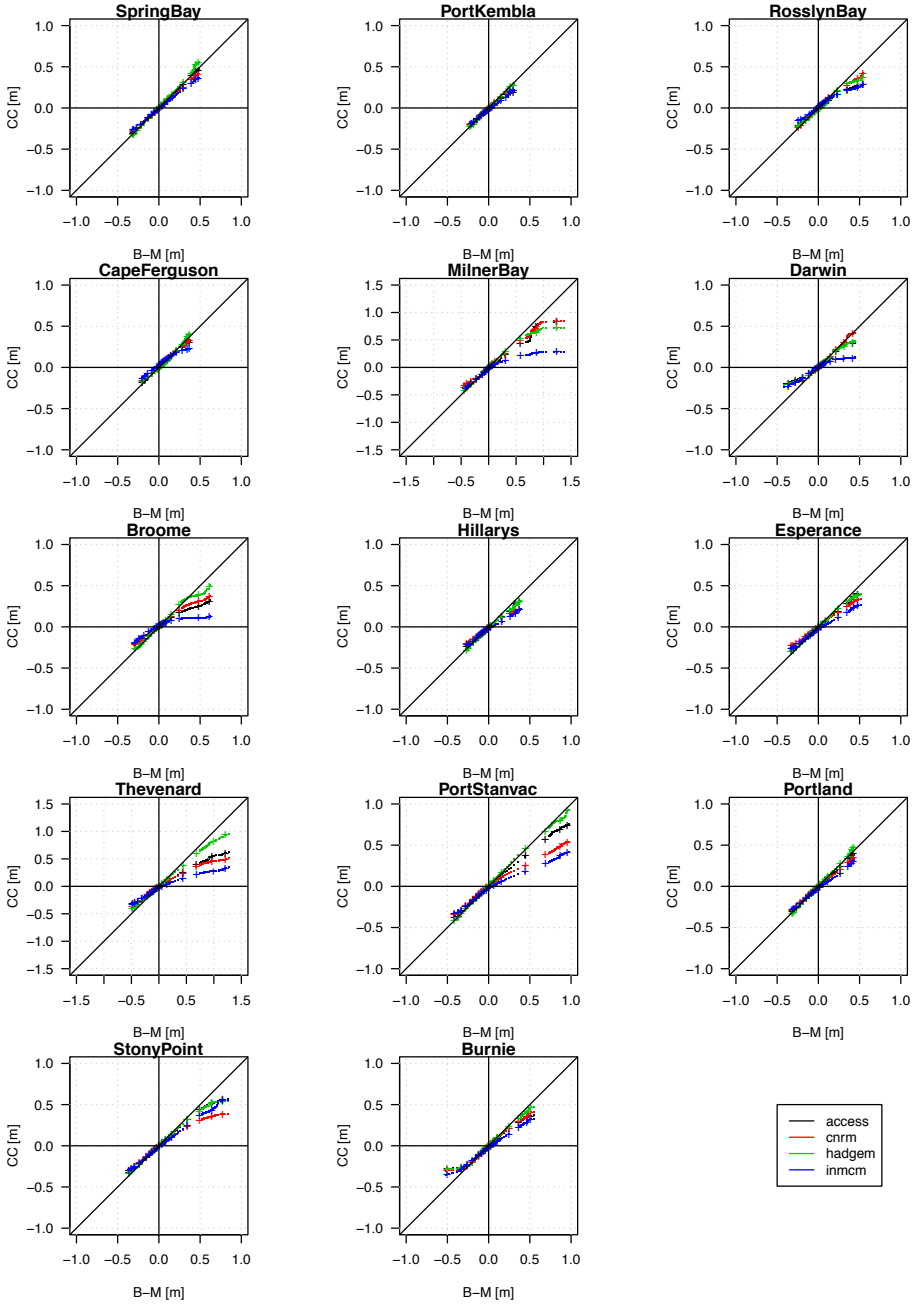

Figure 7: Q-Q plots comparing the sea levels from the four 1980-1999 CC simulations versus the B-M simulation. Note that for clarity only the The '+' symbols are used to denote the 0.1, 1, 10, 50, 90, 99, and 99.9th percentiles.

Nat. Hazards Earth Syst. Sci. Discuss., https://doi.org/10.5194/nhess-2018-64
Manuscript under review for journal Nat. Hazards Earth Syst. Sci.
Discussion started: 26 March 2018

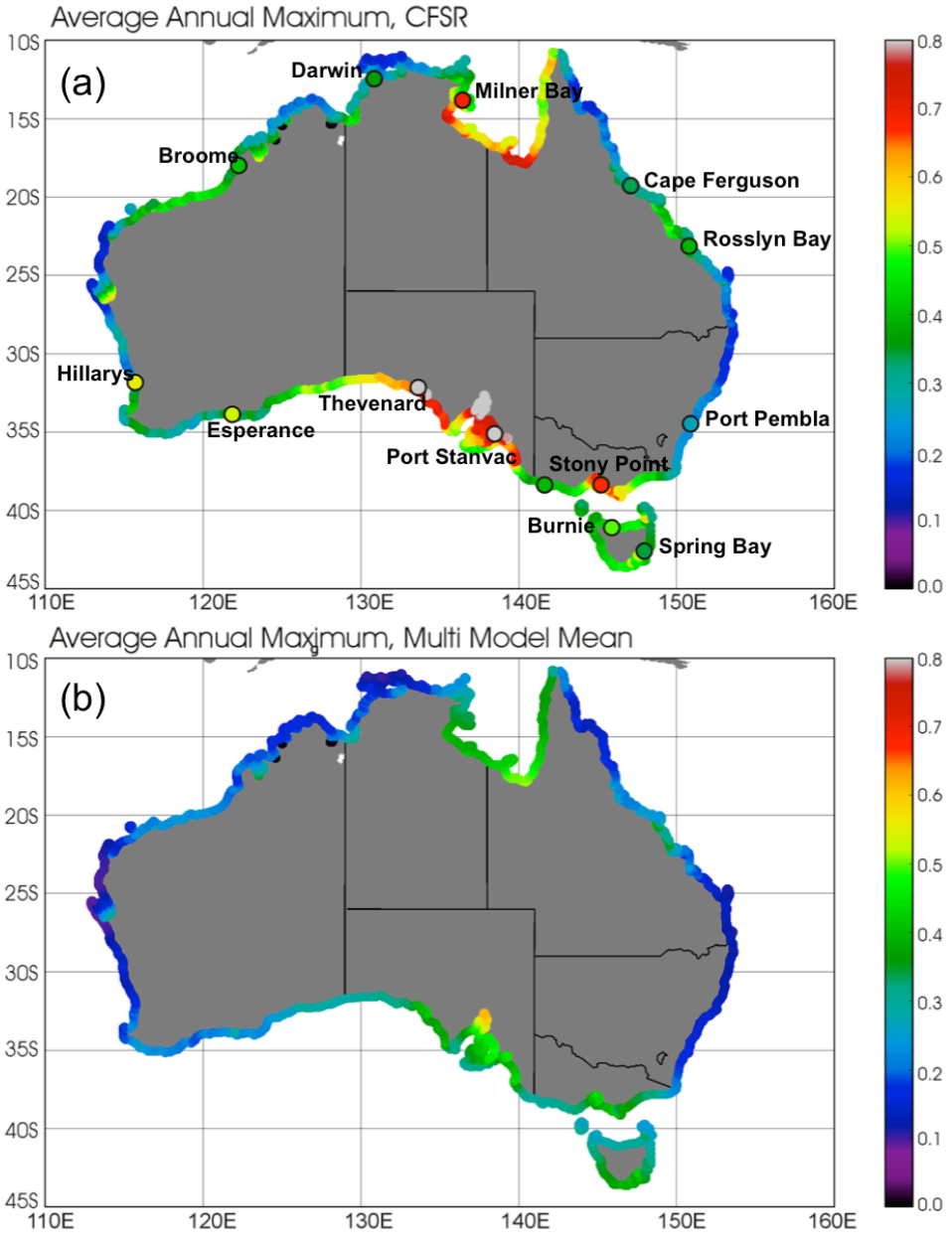

Figure 8: the average annual maximum residual sea level over 1980-1999 from the B-M simulation (top) and the average annual maximum sea level of the four 1980-1999 CC simulations (bottom). The values derived from tide gauges over the period 1993-2012 are shown by the large circles (top). Units are m.

Nat. Hazards Earth Syst. Sci. Discuss., https://doi.org/10.5194/nhess-2018-64
Manuscript under review for journal Nat. Hazards Earth Syst. Sci.
Discussion started: 26 March 2018

Natural Hazards and Earth System Sciences
Discussions

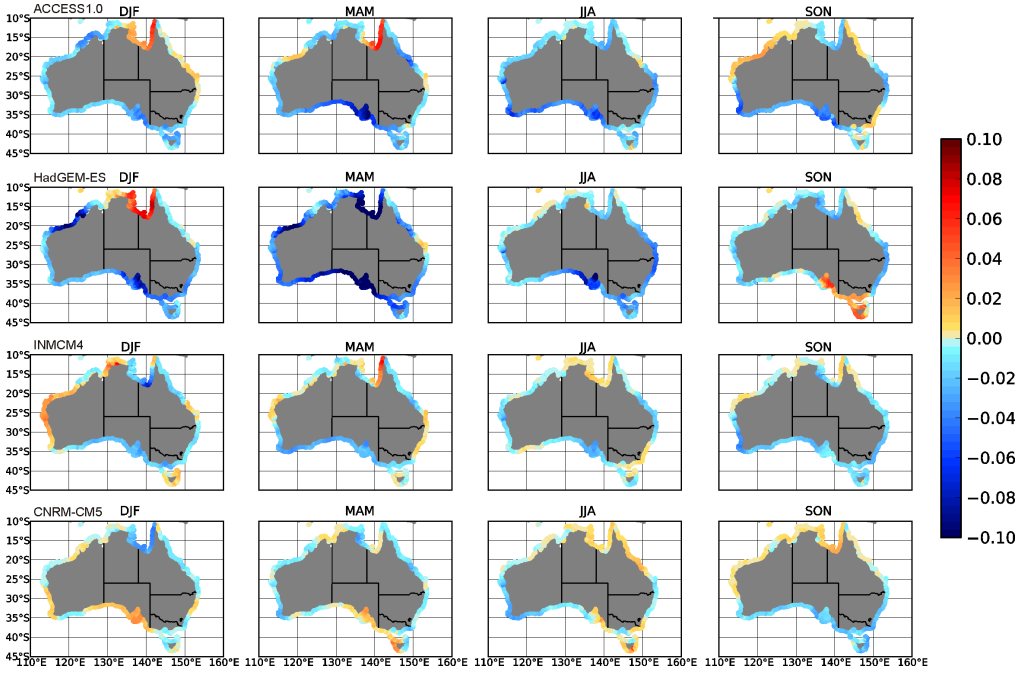

Figure 9: Difference in the average of the seasonal maximum sea level between 2081-2100 and 1981-2000 for the models and seasons indicated.

Nat. Hazards Earth Syst. Sci. Discuss., https://doi.org/10.5194/nhess-2018-64
Manuscript under review for journal Nat. Hazards Earth Syst. Sci.
Discussion started: 26 March 2018

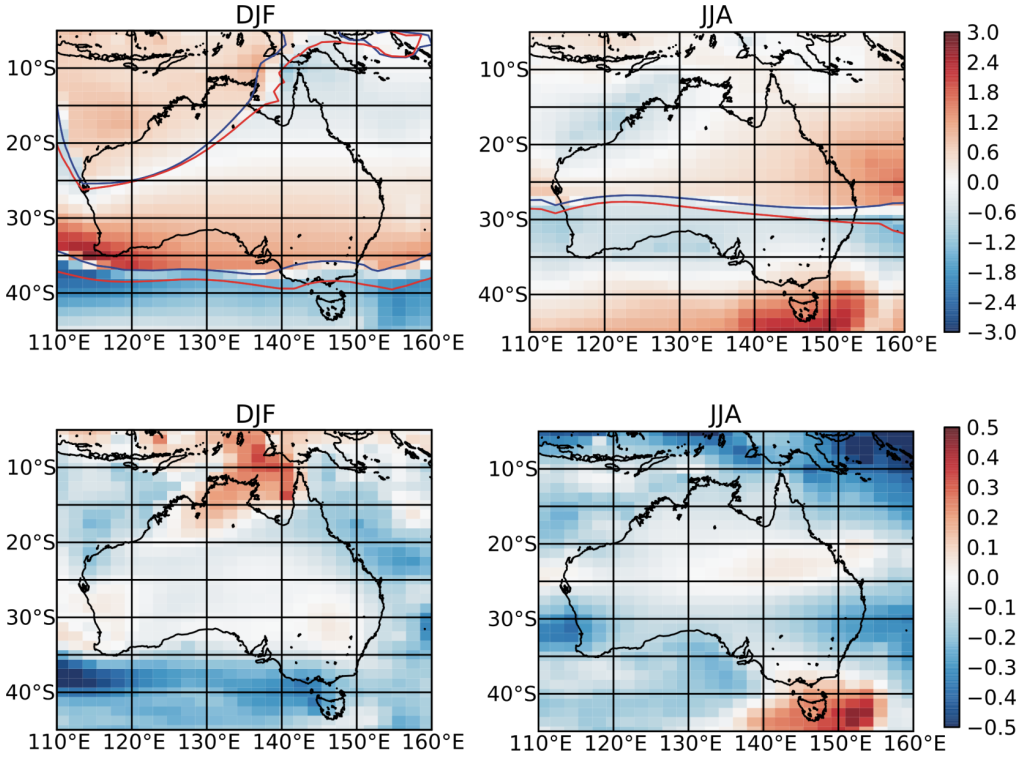

Figure 10: Changes in wind speed (top) for DJF and JJA with zero of zonal wind speed shown as a contour in blue for current climate and red for future climate and (bottom) standard deviation of wind speed for DJF and JJA.

Nat. Hazards Earth Syst. Sci. Discuss., https://doi.org/10.5194/nhess-2018-64
Manuscript under review for journal Nat. Hazards Earth Syst. Sci.
Discussion started: 26 March 2018

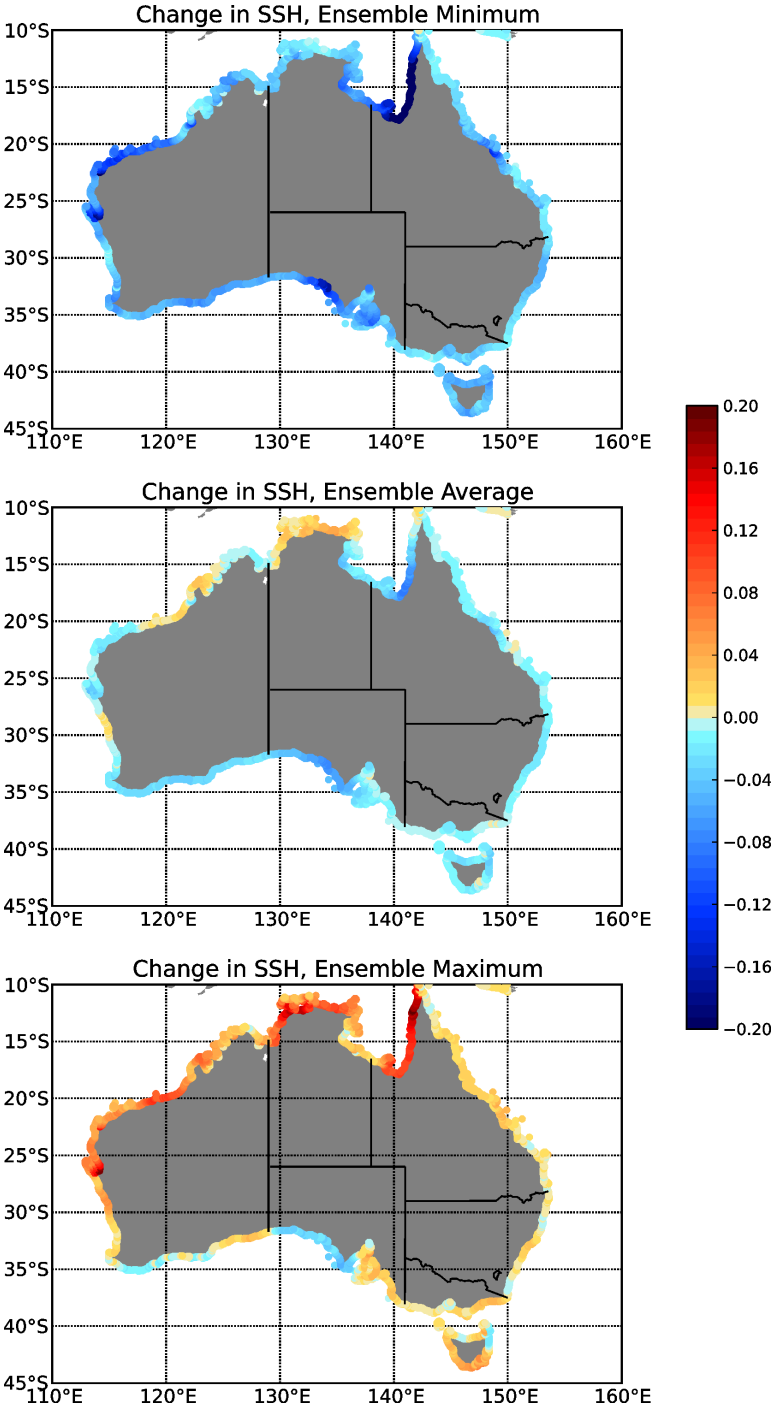

Nat. Hazards Earth Syst. Sci. Discuss., https://doi.org/10.5194/nhess-2018-64
Manuscript under review for journal Nat. Hazards Earth Syst. Sci.
Discussion started: 26 March 2018

Natural Hazards and Earth System Sciences
Discussions

Figure 11: Projected change in the 1 in 20 year average return interval (ARI) extreme sea level (residuals) for the model ensemble. Upper: Ensemble minimum. Middle: Ensemble average. Lower: Ensemble maximum.

5